NIST-GCR-93-637

A COMPUTATIONAL MODEL FOR THE RISE AND DISPERSION OF WIND-BLOWN, BUOYANCY-DRIVEN PLUMES. PART II. LINEARLY STRATIFIED ATMOSPHERE

Xiaoming Zhang and Ahmed F. Ghoniem

Massachusetts Institute of Technology
Cambridge, MA 02139

United States Department of Commerce
Technology Administration
National Institute of Standards and Technology

NIST-GCR-93-637

A COMPUTATIONAL MODEL FOR THE RISE AND DISPERSION OF WIND-BLOWN, BUOYANCY-DRIVEN PLUMES. PART II. LINEARLY STRATIFIED ATMOSPHERE

Xiaoming Zhang and Ahmed F. Ghoniem
Massachusetts Institute of Technology
Cambridge, MA 02139

December 1993

Sponsored by:
U.S. Department of Commerce
Ronald H. Brown, *Secretary*
Technology Administration
Mary L. Good, *Under Secretary for Technology*
National Institute of Standards and Technology
Arati Prabhakar, *Director*

Notice

This report was prepared for the Building and Fire Research Laboratory of the National Institute of Standards and Technology under grant number 60NANB0D1036. The statements and conclusions contained in this report are those of the authors and do not necessarily reflect the views of the National Institute of Standards and Technology or the Building and Fire Research Laboratory.

Prepared for publication at Atmospheric Environment
July, 1993

A COMPUTATIONAL MODEL FOR THE RISE AND DISPERSION OF WIND-BLOWN, BUOYANCY-DRIVEN PLUMES
PART II. LINEARLY STRATIFIED ATMOSPHERE

Xiaoming Zhang and Ahmed F. Ghoniem
Department of Mechanical Engineering
Massachusetts Institute of Technology
Cambridge, MA 02139

Corresponding Author:

Ahmed F. Ghoniem, Professor
Massachusetts Institute of Technology
77 Massachusetts Avenue, Room 3-342
Cambridge, MA 02139
Phone: (617) 253-2295
FAX: (617) 253-5981
email address:ghoniem@mit.edu

Key words; buoyant plumes, vortex simulation, stratified atmosphere.

A COMPUTATIONAL MODEL FOR THE RISE AND DISPERSION OF WIND-BLOWN, BUOYANCY-DRIVEN PLUMES
PART II. LINEARLY STRATIFIED ATMOSPHERE

Xiaoming Zhang and Ahmed F. Ghoniem
Department of Mechanical Engineering
Massachusetts Institute of Technology
Cambridge, MA 02139

Abstract

A multi-dimensional computational model of wind-blown, buoyancy-driven flows is applied to study the effect of atmospheric stratification on the rise and dispersion of plumes. The model utilizes Lagrangian transport elements, distributed in the plane of the plume cross section normal to the wind direction, to capture the evolution of the vorticity and density field, and another set of elements to model the dynamics in the atmosphere surrounding the plume. Solutions are obtained for a case in which atmospheric density changes linearly with height. Computational results show that, similar to the case of a neutrally stratified atmosphere, the plume acquires a kidney-shaped cross section which persists for a long distance downstream the source and may bifurcate into separate and distinct lumps. Baroclinic vorticity generated both along the plume boundary and in the surroundings are used to explain the origin of the distortion experienced by the plume and inhibiting effect of a stratified atmosphere, respectively. The vorticity within the plume cross section forms two large-scale coherent eddies which are responsible for the plume motion and the entrainment. Prior to reaching the equilibrium height, the computed plume trajectory is found to follow the two-thirds law, when extended to include the initial plume size, reasonably well. The entrainment and the added mass coefficients, *0.49* and *0.7*, respectively, are obtained from the numerical results over a wide range of the buoyancy ratio, defined as the ration between the plume buoyancy and the degree of background stratification. In the case of strong stratification, the plume trajectory shows weak, fast decaying oscillations around the equilibrium height. The origin and decay of these oscillations are explained using a simple analytical model.

Nomenclature

B	Buoyancy Ratio;
g	Gravitational acceleration;
h	Spatial discretization length in the plume-air interface;
H	Vertical dimension of the computational domain;
h_s	Spatial discretization length in the stratified background;
H_T	Initial plume height above the ground;
k_v	Added mass coefficient;
N	Brunt-Väisälä buoyant frequency;
N'	Modified buoyant frequency;
R	Square root of the plume cross sectional area;
R_o	Initial Radius of the circular plume cross section;
R_{eq}	Equivalent radius of plume cross section;
R_y	Major (horizontal) axis of elliptical plume cross section;
R_z	Minor (vertical) axis of elliptical plume cross section;
Re_b	Buoyancy Reynolds number;
t	Same as the normalized x coordinate;
U	Homogeneous wind speed;
V	$\equiv \sqrt{\left\|\frac{\rho_p}{\rho_o}\right\| R\, g}$, plume buoyancy velocity;
w	Plume vertical velocity;
x	Horizontal wind direction;
y	Horizontal direction normal to the wind direction;
z	Vertical direction, plume rise;
β	Entrainment coefficient;
ρ_a	Air density;
ρ_o	Reference density;
ρ_p	Plume density apart from reference density;
ρ_s	Background air density apart from reference density;
ξ	Vertical displacement of plume from its equilibrium height;
Δt	Time step;
ε	$\equiv \left\|\frac{\rho_p}{\rho_o}\right\|$, plume mass flux ratio;

Superscript

*	Dimensional quantities.

1. Introduction

The dispersion of strongly buoyant plumes, similar to those generated from massive fires, cooling towers and tall industrial and power plant stacks, in a stable atmosphere is important in many practical applications. Stratification can limit the plume rise and distort its dispersion patterns in ways that worsen its impact on local air quality. Current models (Briggs, 1975) used to describe plume rise and dispersion in a stratified atmosphere, are based mostly on assumptions regarding entrainment and self-similarity and involve several adjustable constants (see Section 3 for a review). Application of computational methods is impeded by the difficulties encountered in the modeling of the buoyancy-generated turbulence, the large numerical diffusion associated with Eulerian discretization schemes, and the computational cost required when dealing with large domains.

A recently developed computational model, based on the Lagrangian interpretation of the dynamics of buoyancy-driven flows, attempts to overcome some of these difficulties (Zhang and Ghoniem, 1993, hereafter referred as Part I). The numerical model utilizes the vortex element and transport element methods to solve the equations governing a wind-blown, buoyancy-driven plume derived directly from Navier-Stokes equations. This paper describes an extension of this model, originally intended for flows in a neutrally stratified atmosphere, to incorporate the effect of atmospheric density stratification on buoyant plume motion. We focus on the case in which the potential density[1] (referred to simply as density) of the air decreases linearly upwards. This form of stratification occurs frequently in elevated layers during the day and in the lowest 100 m or so at night (Briggs, 1975). In a following publication, the effect of an inversion layer will be described in detail.

Atmospheric turbulence may be neglected if one is interested in buoyant plumes not too far away from the emission source, where the plume buoyancy dominates the motion. In general, and depending on how it is generated, there are two types of atmospheric turbulence. The first,

---

[1] Potential density is defined as the density an air parcel would reach if it was brought adiabatically to a standard pressure, which for convenience is usually taken as the pressure at the ground. A neutrally stratified atmosphere is one in which the potential density is constant.

characterized by $\sqrt{\overline{u'^2}}$; where $u' = u - U$ is the fluctuating component of the instantaneous wind velocity, u, around its mean value, U, is due to wind shear instability. On the other hand, the plume buoyancy can be characterized by a buoyant velocity, $V = \sqrt{\left|\frac{\rho_p}{\rho_o}\right| R\, g}$, where ρ_o, ρ_p, R, and g are the reference density, the plume deficient density, the characteristic length of the plume cross section, and the gravitational acceleration, respectively (see Part I). A criterion for neglecting this type of atmospheric turbulence may be given by

$$\frac{V}{\sqrt{\overline{u'^2}}} = \sqrt{\left|\frac{\rho_p}{\rho_o}\right| \frac{R\, g}{\overline{u'^2}}} >> 1. \qquad (1)$$

The second type of atmospheric turbulence is associated with the convective instability due to the uneven heating of air parcels in the atmosphere. A velocity scale representing the intensity of this turbulence over a horizontal distance equal to the plume size is given by $\sqrt{\left|\frac{\Delta\rho_a}{\rho_o}\right| R\, g}$, where $\Delta\rho_a$ is the scale of air density variation over a horizontal distance R. A corresponding criterion for neglecting this convective atmospheric turbulence is thus

$$\left|\frac{\rho_p}{\Delta\rho_a}\right| >> 1. \qquad (2)$$

In this paper, we neglect atmospheric turbulence and focus on plume rise and dispersion due to buoyancy and buoyancy-generated turbulence in a stratified atmosphere (the effect of the former will be incorporated in future efforts). In Section 2, we describe the physical mechanism of baroclinic-vorticity generation in buoyant flows, and summarize how atmospheric stratification is implemented in our model. In Section 3, we review the integral models which have been developed to characterize the plume trajectory, and refer to field observations on plume dispersion in a linearly stratified atmosphere. In Section 4, we present the computational results in the form of the plume trajectory and dispersion pattern, and compare our results with experimental data. An algebraic formula for the plume rise is obtained by modifying the classical two-thirds power law. The adjustable empirical constants in the formula: the entrainment coefficient, and the added mass coefficient are calibrated using the numerical results.

The paper ends with a brief conclusion in Section 5, and a note on plume motion near its equilibrium height in the Appendix.

2. Background

2.1. Vorticity Generation in a Disturbed Stratified Atmosphere

Dynamically, plume rise and dispersion in a weakly turbulent atmosphere is driven by the potential energy of the plume material. Kinematically, the plume motion is driven by the vorticity generated due to the density difference between the plume material and the surrounding air (see Part I for detail). The latter view has the advantage of allowing one to describe the turbulence generated within the plume cross section as well. To simplify the following discussion, we use the Boussinesq approximation which, in our previous work, has been shown to be accurate when the relative density perturbation is less than 0.1. With this approximation, baroclinic vorticity is generated only where a finite horizontal density gradient exists, i.e. along the distorted plume-air interface which at high Reynolds number, remains confined to a small subset of the entire domain. We also assume, as in Part I, that the density distribution inside the initial plume cross section is uniform. The effects of density non-uniformity within the plume cross section, which is expected to be of secondary importance, will be investigated in the future.

In the presence of atmospheric density stratification, as the plume rises, the initially horizontal density isolines in the background are distorted. A density field with non-zero horizontal gradient component is thus established, and baroclinic vorticity is generated in the atmosphere. This is illustrated schematically in figure 1 for a crosswind section of a rising plume in a continuously stratified, stable atmosphere. As shown in the figure, vorticity generated in the background induces a net downward motion on the plume in the direction opposite to the flow induced by the vorticity generated due to the plume's own buoyancy. Eventually, the plume reaches a terminal, equilibrium, or level-off height where the effect of the background vorticity balances that of the vorticity around its surface. Occasionally, the plume may experience weak, fast decaying oscillations around this height (Briggs, 1975) due to a mechanism that will be discussed later. It should be noted, as will be shown later, that even after the plume reaches its

equilibrium height, vorticity generated both at the plume surface and in the surroundings still plays an important role in dispersing its material.

2.2. Model Formulation and Numerical Implementation

The partial differential equations governing the flow of a steady, three-dimensional, wind-blown, buoyancy-driven plume were presented in Part I. Incorporating the atmospheric density stratification in the formulation does not change the governing equations, except for the fact that vorticity can now be generated in the background and its induced field must be incorporated in the solution.

In principle, in a continuously stratified atmosphere, we must discretize the entire space since non-zero horizontal density gradients could be established everywhere. However, the plume induced motion, and thus the distortion of the background, decays rapidly away from the plume center[2]. Moreover, the far field effect on the plume motion is generally negligible, see Section 4.1. Thus, to account for vorticity generated in the atmosphere noting that the air density isolines remain almost horizontal in the far field, we need only consider an area several plume characteristic length, R, around the plume center . Furthermore, in practice, the density gradient in the background is much smaller than that across the plume-air interface. Thus, we discretize the background density field into transport elements whose size is larger than the size of the elements used to discretize the plume-air interface. The discretization is schematically illustrated in figure 2. The choice of two different sizes of elements reduces the computational load while maintaining the numerical accuracy.

---

[2] Note that the distortion of the atmospheric density isolines, induced by the plume vorticity, is proportional to the velocity gradient, $\Delta u \approx \frac{\Gamma}{r^2}\Delta r$, where Γ is the circulation and r is the distance away from the vorticity center, i.e., the effect of vorticity induced distortion decays as the square of the distance away from the center of the vorticity.

3. Review

Plume rise in a linearly stratified atmosphere has been analyzed in the literature. Denoting the reference density, taken here as the air density at the height of the plume source, by ρ_o, we write the density distribution as

$$\rho = \begin{cases} \rho_o + \rho_p(t,y,z) & \text{inside the plume} \\ \rho_o + \rho_s(t,y,z) & \text{outside the plume} \end{cases} \qquad (3)$$

where ρ_p and ρ_s are the density perturbation of the plume and the air, respectively. The background stratification is characterized by the Brunt-Väisälä frequency, $N^2 = -\frac{g}{\rho_o}\frac{d\rho_s}{dz^*}$. As it rises, the plume entrains denser air until it reaches an equilibrium height where its average density is close to that of its surroundings. Meanwhile, the plume spreads out horizontally and vertically. The trajectory of a point source plume between the source and a point close to the level-off height has been described by the two-thirds power law (Briggs, 1969, 1975, Fay, 1973, Weil 1988). In a uniform wind with speed U, the trajectory of a buoyant plume generated from a finite size source can be obtained using the same procedure as in the derivation of conventional two-thirds power law after modifying the initial conditions to account for the finite initial plume size. The derivation follows Weil's (1988) and is similar to that described in Part I of this study. The resulting expression of the plume rise z^* is:

$$z^* = \frac{1}{\beta}\left\{\left[\frac{3\beta F_b}{(1+k_v)N'^2U}\left(1-\cos\frac{N' x^*}{U}\right)+R_o^{*3}\right]^{1/3} - R_o^*\right\} \quad \text{for} \quad \frac{N' x^*}{U} \le \pi \qquad (4)$$

where R_o^* is the radius of the initial plume cross section, k_v is the "added" or "virtual" mass coefficient which accounts for the momentum of the ambient fluid displaced by the plume as the latter rises and of the small scale motion inside the plume; $N' = N/(1+k_v)^{1/2}$ is a modified buoyancy frequency which takes k_v into account; β is an entrainment coefficient used to describe the growth of the plume radius due to entrainment[3]; and $F_b = R_o^{*2}\, Ug\left|\frac{\rho_p}{\rho_o}\right|$ is the buoyancy flux.

---

[3] Weil (1988) used a modified entrainment rate related to the added mass coefficient in his derivation.

The constants in equation (4) have been obtained using laboratory experiments and field observations of point-source plumes. However, as pointed out by Turner (1986), this two-thirds power "law" fails near the level-off region because the entrainment and similarity assumptions used in its development become invalid. Similar reasons, coupled with the difficulty in defining the plume center and the size of its cross section in different experiments (List 1982, Gebhart et al, 1984), have been used to describe the origin of the following unresolved problems:

(1) Good correlation between the two-thirds power law and different experiments are achieved by adjusting the entrainment coefficient for each case, i.e., the coefficients are not truly universal. From laboratory experiments, Slawson and Csanady (1967) found $\beta = 0.43$, while Hewett et al. (1971) got the best fit with $\beta = 0.71$. From field experiments, Hoult et al (1969) found that $0.3 < \beta < 1.0$, while Fay et al. (1970) obtained $0.5 < \beta < 2.0$.

(2) In models which assume that the plume cross section remains circular, the radius increases with the plume rise as

$$R^* = R_o^* + \beta z^* . \qquad (5)$$

Using data from the same experiment to fit the trajectory, equation (4), or the radius, equation (5), Briggs (1975) found $\beta = 0.6$ or 0.4, respectively. This inconsistency was also observed by other authors; Weil (1982) obtained $\beta = 0.6$ from the trajectory data while $\beta = 0.5$ from the radius data.

In the early development of the two-thirds power law, the added mass coefficient, k_v, was not included (Briggs, 1969, Fay et al, 1970). Later k_v was introduced (Briggs, 1975, Weil, 1988) to improve the accuracy of the trajectory law derived from the integral formulation. The added mass concept was originally developed for a solid body accelerating in a fluid (Yih, 1977) to account for the work done to increase the momentum of the ambient fluid. In the case of a circular cylinder moving in an inviscid flow, $k_v = 1$. The same value is usually suggested for plumes where the driving force is buoyancy. However, the actual value may deviate from unity since the plume is not a solid body and its cross section is not circular. If fact, the plume cross section, as shown in Part I, is shaped in the form of an inverted kidney which evolves as the

plume rises. Furthermore, not only a significant portion of surrounding air is induced into motion due to the presence of the plume, but also motion at scales smaller than the plume radius is developed within its cross section. In practice, k_v can be regarded as merely another empirical constant whose value should be adjusted to make the two-thirds power law fit the experimental trajectory better.

The shape of the plume cross section is an important feature of plume dispersion, especially for large-scale, strongly buoyant plumes. As the plume rises, two counter-rotating vortices, which divide the plume material into two lumps, are generated. Plume bifurcation is a frequently observed yet not well understood phenomenon. Some of the laboratory and field experiments describing this bifurcation have been reviewed in Part I. Here we cite three more experiments, which have been documented carefully, in which bifurcation have been cited. The first is the fire plume experiment of Church et al (1980), conducted for the purpose of investigating the mechanism leading to the formation of large-scale vortices in fire plumes. These authors hypothesized that the generation of a double-vortex structure is due to the tilting and stretching of the vorticity originally associated with background wind shear, and the vorticity generated within the plume by the action of buoyancy and drag forces. The second is the Lidar measurements of cooling tower plumes (Hawley, 1985, Bennett et al, 1992). Sykes et al (1986) suggested that the interaction between the crosswind and the initial vertical momentum of the plume may be the cause for the bifurcation. The third experiment is the laboratory water plume model of Alton et al (1993). Clearly, the mechanism leading to plume bifurcation requires further investigation (Zhang and Ghoniem, 1993).

4. Numerical results

4.1. Entrainment, added mass and plume trajectory

The notations and normalization procedure used in this paper are the same as those employed in Part I. To characterize the background in which the plume disperses, we define the buoyancy ratio as the ratio between the plume buoyancy to the degree of stratification,

$$B = \frac{V^2}{N^2 R^2} = \frac{\varepsilon g}{N^2 R} \tag{6}$$

where $\varepsilon = \left|\frac{\rho_p}{\rho_o}\right|$ is the plume deficient mass flux ratio and R is the plume length scale, taken as the square root of the initial plume cross sectional area. In terms of the buoyancy ratio, equation (4) becomes

$$z = \frac{1}{\beta\sqrt{\pi}} \left\{ \left[3\sqrt{\pi}\,\beta B \left(1 - \cos \frac{x}{\sqrt{(1+k_v)B}} \right) + 1 \right]^{1/3} - 1 \right\}, \tag{7}$$

where the effects of plume buoyancy and background stratification have been grouped into a single dimensionless parameter[4], B. In terms of the variables defined above, the buoyancy ratio can be written as

$$B = \frac{\left|\frac{\rho_p}{\rho_o}\right| g}{-R\frac{g}{H}\frac{\rho_{st} - \rho_{sb}}{\rho_o}} = \frac{|\rho_p| R}{(\rho_{sb} - \rho_{st})H} \tag{8}$$

where ρ_{sb} and ρ_{st} are the air densities at the bottom and top boundaries of the computational domain, and H is the vertical dimension of this domain, as shown in figure 2. For typical low-level atmospheric stratification, $\left|\frac{\rho_{sb} - \rho_{st}}{\rho_o}\right| \approx 10^{-3}$ over a vertical range of $H = O(100m)$. If the

---

[4] The steady motion of a plume with initial circular cross section in a uniform wind, U, depends on four independent dimensional variables: R, g, ρ_p, and $\frac{\partial \rho_s}{\partial z^*}$. Only one dimensionless parameter can be formed from these four variables is, $B = \frac{\rho_p / R}{\partial \rho_s / \partial z^*}$.

plume size is of $R = O(10m)$, and with deficient density $\left|\frac{\rho_p}{\rho_o}\right| \approx 10^{-2}$, the corresponding buoyancy ratio is $B = 100$. For large plumes, the expected range of the buoyancy ratio is $10 < B < 1000$.

We ran the computational code for four values of the buoyancy ratio, $B = \infty, 50, 25$, and 12.5, ranging from neutral to strong stratification, with all other conditions: the initial plume size $(R_y, R_z) = (\frac{1}{\sqrt{\pi}}, \frac{1}{\sqrt{\pi}})$, the initial deficient plume density $\frac{\rho_p}{\varepsilon\rho_o} = -1.0$, the initial height $H_T/R = 23.0$, and the buoyancy Reynolds number $R_{eb} = 1000$, being the same. Symmetry across the plume centerline was enforced at all times. The discretization lengths for the computational elements is $h/R = 0.025$ for the plume-air interface, and $h_s/R = 0.5$ in the stratified atmosphere, as shown in figure 2. The marching step in the wind direction is $\Delta t = 0.025$[5]. The vertical extent of the domain is $15 \le z \le 40$, so that $H/R = 25$. The horizontal extent is $0 \le y \le 7.09$. The computational results were used, besides investigating the fundamental dynamics governing plume rise and dispersion, to determine the values of the entrainment coefficient and the added mass coefficient in the trajectory formula, equation (7). It should be noted that the values of these constants may vary with B. Similar to Part I, we define the plume height at any downwind location as the algebraic mean of the maximum and minimum heights of the plume cross section.

The computed plume center height of each case was fitted to the trajectory formula by adjusting the arbitrary constants, β and k_v. The computed trajectories of the four cases, and the corresponding fitted curves are shown in figure 3. The best fit for all four cases were obtained using the following pair of constants: $\beta = 0.49$ and $k_v = 0.7$. It was found that while β had a stronger influence on the equilibrium height, k_v affected the downwind distance where the equilibrium height was reached. As mentioned earlier, equation (7) is expected to be valid only for the part of the trajectory prior to reaching the level-off height.

The top curve in figure 3 corresponds to the case of plume rising in a neutrally stratified atmosphere. In this case, the plume rises continuously and there is no equilibrium height.

---

[5] In terms of the parameters used to check the convergence of the computations, such as the plume trajectory, numerical results with smaller values of h, h_s and Δt are indistinguishable from the results described in this paper.

Equation (7) describes this curve using $N^2 = 0$, $\beta = 0.7$, and $k_v = 0$, as shown in Part I. Therefore, the same trajectory can be represented by the two-thirds law using two different sets of constants; one with the a finite added mass coefficient and the other without[6].

The lowest curve in figure 3, where the plume reaches the equilibrium height early, corresponds to a case with strong stratification. Weak, fast decaying oscillations are observed in the level-off region. This is consistent with the experimental observations that the plume oscillations decay rapidly in the downwind direction (Briggs, 1975). Plume oscillations are generated as the buoyant plume overshoots its equilibrium height and disturbs the initially calm background. These oscillations, which possess a well-defined frequency, then travel through the atmosphere in the form of gravity waves due to the restoring action of the stratified background. A detailed discussion on the origin and the character of these oscillations is provided in the Appendix using a simple analytical model. The intermediate cases also follow the extended two-thirds law well until the plumes reach their corresponding equilibrium heights, where the analytical curves overestimate the heights. As expected, the trajectory formula (4) generally cannot predict the maximum plume rise.

Part of the kinetic energy associated with the plume motion, transformed from its initial potential energy through the vorticity, is radiated away in the crosswind section via the internal waves. Thus, a significant part of the surrounding air may be disturbed and a larger computational domain may be needed to capture the effect of these waves. To find out the effect of the finite domain size on the results, we repeated the calculation of the $B = 25$ case after

---

[6] Briggs (1969) proposed using $\beta=0.4$ in the formula for the plume radius, equation (5), and $\beta=0.6$ in the trajectory formula, equation (4). This means that, in the analytical model used to derive the two-thirds law, $R = R_o + 0.6\, z$ is used to evaluate the plume momentum, while $R = R_o + 0.4\, z$, is used to evaluate the plume size. Using larger values of R in calculating the momentum may account for part of the momentum of the background fluid which is set in motion by the plume. Thus, it is not surprising that the early version of the two-thirds law, which did not incorporate the concept of added mass, could still describe the plume trajectory well (Fay et al, 1970, Hewett et al, 1971).

doubling the horizontal extent of the computational domain to $y = 14.18$. No significant changes were observed in the result up to $x = 17.5$ where the calculations were terminated.

Now we compare the entrainment relation expressed by equation (5) with the simulation results. In dimensionless form, if we use the equivalent radius[7] to describe the size of the plume cross section, equation (5) can be written as

$$R_{eq} = 1/\sqrt{\pi} + \beta z \qquad (9)$$

Figure 4 shows the computed equivalent radius as a function of the plume rise. Clearly, the growth of the plume cross section depends weakly on the buoyancy ratio before reaching the level-off height. Beyond $z=2$, and before the level-off distance, the computed equivalent radius grows almost linearly with height. Both equation (9) and its corresponding form for a point-source plume, $R_{eq} = \beta z$, are shown using $\beta = 0.49$ which was obtained from the trajectory. As shown in the figure, equation (9) overestimates the equivalent radius, although the slope is reasonably captured. Beyond $z=2$, the equivalent radius increases with height as if the plume had started from a virtual point source at $z=0$.

It is interesting to note how the buoyancy ratio affects the plume spread close to the level-off height. In the neutrally stratified case, $B = \infty$, the equivalent radius and the plume rise increase indefinitely. In the weakly stratified case, $B= 50$, the radius continues to expand after the plume reaches the level-off region. In the cases with stronger stratification, $B= 25$ and 12.5, the plume radius and rise are curtailed beyond the equilibrium height, as shown by the crowd of points near the level-off height.

4.2. Other integral characteristics of the plume

To investigate the effect of stratification on plume dispersion, we plot the evolution of the vertical and horizontal widths of the plume cross section, both as defined in Part I. Figure 5 shows that beyond the level-off height, the vertical width of the plume cross section increases in

[7] The equivalent radius is defined as the radius of the circle whose area the same as the actual plume cross-sectional area.

the neutrally stratified case, oscillates around a nearly constant value in the weakly stratified atmosphere, and decreases in the strongly stratified atmosphere. Achieving an almost constant vertical width under conditions of intermediate stratification is consistent with experimental results (Briggs, 1975). The decrease of the vertical width under strong stratification is because while the top side of the cross section is capped, the bottom side continues to rise, as will be seen in more detail in the next section. On the other hand, as shown in figure 6, the plume horizontal width increases continuously, with the rate of expansion being approximately the same for all cases. Thus, atmospheric stratification affects the plume dispersion mainly by suppressing the vertical fluid motion.

As mentioned earlier, the effect of atmospheric stratification can be understood in terms of the vorticity generated in the background, as presented in figure 1. During the early stages, negative vorticity (on the right side of the centerline), which lifts the plume upwards, is generated at the interface between the plume and the surrounding. In the later stages, after the atmosphere has been disturbed, positive vorticity (on the same side), which tends to push the plume downwards, is generated in the stratified background. Using the results of the simulation, we can probe into this mechanism in more detail. Figures 7 and 8 show the total circulation, integrated over half of the computational domain, in the plume-air interface and in the background, respectively. Initially, and in all cases, the magnitude of the total circulation at the plume-air interface increases rapidly at a rate which is independent of B. However, The terminal value of the total circulation in the plume cross section is a function of B. The saturation of the total plume circulation is due to the reason described in Part I: both negative and positive circulation grows at the same rate following the large eddy roll-up stage. On the other hand, after the atmosphere has been disturbed, the positive background circulation increases continuously. The stronger the stratification, the faster the rate at which ambient circulation is generated. With strong stratification, the magnitude of the positive background circulation could be larger than that of the negative plume circulation. However, the induced motion by the former

is not necessarily stronger because this positive background circulation is distributed over an area much larger than the plume cross section, as will be shown in the next section.

The deformation of the plume cross section can also be measured in terms of the growth of the boundary (interface) length between the plume and the surrounding atmosphere. The plume circumference, shown in figure 9, exhibits exponential growth following a short acceleration period with a high rate during the early large eddy roll-up stage and a lower rate during the small eddy roll-up stage. It is interesting to note that this circumference grows continuously beyond the point where the plume has reached a level-off height. This means that the buoyancy-generated turbulence still plays an important role in dispersing the plume material even at this later stage. The figure shows that the growth of the circumference is almost independent of the background stratification.

The plume equilibrium, or level-off, height, z_{eq}, is an important quantity. This height is commonly used in conventional models as the terminal rise of a buoyant plume in the presence of atmospheric stratification. At this height, the plume material is assumed to be distributed according to a Gaussian distribution. Figure 10 shows the plume terminal rise as a function of the buoyancy ratio (two additional cases, $B = 16.67$ and 33.3, were computed to establish this curve). In practice, it is customary to use equation (4) to calculate the maximum plume height and multiply the result by an empirical factor to obtain the final equilibrium height. This, however, may not always be appropriate due to the following reasons: (a) the plume trajectory formula, equation (4), does not predict an accurate maximum plume height since the entrainment and similarity assumptions become invalid near this region; (b) the empirical multiplication factor is not a well defined quantity; and (c) the experimental results on point source buoyant plumes still involves fairly large uncertainties.

4.3. Concentration and vorticity distributions

Figure 11 shows the deficient density distribution across the plume cross section at successive downwind distances for the case of $B = 12.5$. The increment between the density

isolines is the same in each cross section and decreases for larger downwind distance. The number of isolines in the background increases for larger x because, while the number of isolines are the same in each section, the range of density variation decreases. Initially the plume cross section is circular (only half of the section is shown) and the background stratification is horizontally uniform, so that the background density isolines are all horizontal. Due to buoyancy, a double-vortex structure, which induces the upwards motion and deforms the plume cross section into a kidney-shaped pattern, is generated. Concomitantly, the initially horizontal background density isolines are disturbed and positive background vorticity (on the same half of the plume) is generated.

Beyond $x=7$, each side of the cross section splits into two lumps with more material being associated with the lower lump. Both lumps continue to rise until the plume center reaches its equilibrium height at $x=12$. Thereafter, the top lump stays almost at a fixed height while the lower one continues to rise slowly thus decreasing the overall vertical width of the plume. This bifurcation phenomenon was also observed in the two-dimensional thermal experiment of Tsang (1971).

Figures 12 and 13 show contours of: (a) the plume deficient density, which is proportional to plume material concentration, $\frac{\rho_p}{\epsilon\rho_o}$; (b) the vorticity; (c) the background deficient air density, $\frac{\rho_s}{\epsilon\rho_o}$; and, (d) the velocity field in the cross-wind section at $x = 4$ and $x = 14$, respectively, all for the strongly stratified case with $B= 12.5$. Since we have used separate transport elements for the plume perturbation density and air density, these two fields can be calculated and presented separately here.

At $x = 4$, the plume cross section exhibits the kidney shaped structure which was also observed in the neutrally stratified case (Part I). At this section, located only a short distance away from the source, negative vorticity is generated over a large portion of the plume-air interface, as demonstrated in figure 1. The cumulative action of this vorticity is to propel the plume upwards. Meanwhile, positive vorticity is generated in the surrounding, although its effect on the plume trajectory is not yet noticeable, see figure 3. The mechanism of positive

vorticity generation in the surrounding atmosphere can be explained using figure 12c which exhibits the density isolines in the immediate vicinity of the plume. Heavy air from lower altitudes is entrained into the core, and is displaced by lighter air which flows downwards from higher altitudes along the plume sides. This imparts strong curvature on the background density isolines and leads to the generation of positive vorticity. The velocity field, shown in figure 12d, depicts a structure which can be attributed to a vortex dipole, coincident with the plume material concentration contours. At $x = 14$, and according to figure 3, the plume is at the level-off region. On each side of the centerline, the plume breaks up into two lumps with the lower one containing more of the original plume material. The break-up of a plume into several lumps has been observed by Richards (1963) and is considered to be one of the important mechanisms of turbulent plume dispersion.

The vorticity field in figure 13b shows two eddies: the lower eddy having strong negative circulation and the upper eddy having weak positive circulation (The sense of rotation of these eddies is confirmed by figure 13d). The positive background vorticity is distributed over a much larger area than that occupied by these two plume eddies. Since the plume is not rising at this stage, the net effect of these eddies on its trajectory must be balanced by the effect of the positive vorticity generated in the background. According to the conventional argument, the plume reaches the level-off height when its average density, being that of the original plume material after getting diluted by the entrained air, is the same as the local atmospheric density. This "dynamic" argument, however, relies on quantities, such as the plume size, which are difficult to define. Our "kinematic" argument is based solely on the motion induced by the vorticity generated within the plume cross section and in the background.

The background density field in figure 13c illustrates the effect of the plume break-up on the motion of surrounding air. In the early stages, air, which is heavier than the plume material, is entrained vertically upwards into the core. At $x=14$, the entrained air is forced to move horizontally away from the centerline, indicating that the plume has stopped its vertical ascent

and is spreading out horizontally. Meanwhile, some of the heavier air in the plume core is leaking downwards.

The velocity field, depicted in figure 13d, depicts the manifestation of the complex vorticity structure within and in the immediate vicinity of the plume. As mentioned earlier, the vorticity field is composed of a positive eddy on the upper side and a negative eddy on the lower side of the plume cross section. Near the center, $y=0$, the flow induced by this vorticity distribution acts to dislodge some of the air entrained earlier. It is important to add at this point that even after reaching the level-off height, the plume continues to disperse horizontally due to the action of the large scale vortices.

5. Conclusion

The computational plume model, which is based on the utilization of the transport element method to solve the equations governing a buoyant flow in a horizontal uniform wind, has been extended to include the effect of atmospheric density stratification. Results have been obtained for a wide range of the buoyancy ratio which characterizes the relative importance of the plume buoyancy to the change in the atmospheric density. The computed plume trajectory and dispersion patterns have been compared with experimental measurements whenever possible. The extended two-thirds power law is found to describe the plume trajectory reasonably well before the plume reaches its equilibrium height. The entrainment and the added mass coefficients are found to be $\beta = 0.49$ and $k_v = 0.7$, over a wide range of buoyancy ratio.

The computational results suggest that the plume cross section first changes from a circular into a kidney-shaped form, and then breaks up into several lumps at later stage. This behavior has been confirmed qualitatively by various field and laboratory observations. However, quantitative measurements of the plume material distribution, which can be used in direct comparison with the numerical results, are currently scarce. This problem may be overcome using the newly developed rapid-scanning Lidar technique which is capable of obtaining the instantaneous density distribution within the plume cross section (Bennett et al, 1992). Application of this technique may provide considerable field data to guide further model validation.

Many features of buoyant plume motion, e.g., the kidney-shaped cross section, the induced motion of the surrounding air and the inhibiting effect of atmospheric stratification, can be attributed to the buoyancy-generated vorticity. This turbulence, being neither homogeneous, nor isotropic or stationary, occurs often in fluid motion with finite density gradient. This vorticity exhibits itself in the form of a long-preserved, large-scale, coherent vortex structure, which governs the entrainment process. Since this turbulence is frequently encountered in nature, its understanding and proper description is important both fundamentally and practically.

The agreement between the simulated results and the experimental observations shows the potential for applying the model to more complicated problems, such as, plume interaction with an inversion layer, heavy particle separation from buoyant plumes, and chemically reactive plume dispersion. Neglected from the current model are the initial momentum and/or shear in the plume section. Ways of modeling their effects are currently being investigated

Acknowledgment

This work has been jointly supported by the Mineral Management Services of the Department of the Interior, and the Building and Fire Research Laboratory of the National Institute of Standards and Technology. The computer support for this project is provided by the Illinois National Center for Supercomputer Applications.

References

Alton B. W., Davidson, G. A. and Slawson, P. R. (1993) Comparison of measurements and integral model predictions of hot water plume behavior in a crossflow, *Atmos. Environ.* **27A**, 589-598.

Bennett M., Sutton, S. and Gardiner, D. R. (1992) An analysis of Lidar measurements of buoyant plume rise and dispersion at five power stations, *Atmos. Environ.* **26A**, 3249-3263.

Briggs G. A. (1969) *Plume rise.* USAEC Critical Review Series, TID-25075, NTIS, 81pp.

Briggs G. A.(1975) Plume rise predictions. *Lectures on Air Pollution and Environmental Impact Analysis*, D. A. Haugen, Ed., Amer. Meteor. Soc., Boston, 59-111.

Church C. R., Snow, J. T. and Dessens J. (1980) Intense Atmospheric vortices associated with a 1000 MW fire. *Bull. Am. Meteorol. Soc.*, **61**, 682-694.

Fay J. A., Escudier M. P. and Hoult D. P. (1970) A correlation of field observations of plume rise. *Journal of Air Pollution Control Association,* **20**, No.6, 391-397.

Fay J. A. (1973) Buoyant plumes and wakes, *Ann. Rev. of Fluid Mech.*, **5**, 151-160.

Gebhart B., Hilder D. S. and Kelleher M. (1984) The diffusion of turbulent buoyant jets. *Int. J. Heat Mass Transfer*, 1-57.

Hawley J. G. (1985) Plume model validation and development project: differential absorption Lidar measurements of SO_2 in moderately complex terrain. EA-3758, Research Project 1616-12, SRI international, 333 Ravenswood Avenue, Menlo Park, California 94025.

Hewett T. A., Fay J. A. and Hoult D. P.(1971) Laboratory experiments of smokestack plumes in a stable atmosphere, *Atmos. Environ.* **5**, 767-789.

Hoult D. P., Fay J. A. and Forney L. J. (1969) A theory of plume rise compared with field observations, *Journal of Air Pollution Control Association,* **19**, No.8, 585-590.

List E. J. (1982) Turbulent jets and plumes, *Ann. Rev. Fluid Mech.*, **14**, 189-212.

Richards J. M. (1963) The penetration of interface by cylindrical thermals, *Quart. J. Roy. Meteor. Soc.*, **89**, 254-264.

Slawson P. R. and Csanady G. T. (1967) On the mean path of buoyant, bent over chimney plumes, *J. Fluid Mech.* **28**, 311-322.

Sykes R. I., Lewellen, W. S. and Parker S. F. (1986) On the vorticity dynamics of a turbulent jet in a crossflow. *J. Fluid Mech.*, **168**, 393-413.

Tsang G. (1971) Laboratory study of line thermals. *Atmos. Environ.*, **5**, 445-471.

Turner J. S. (1986) Turbulent entrainment: the development of the entrainment assumption, and its application to geophysical flows, *J. Fluid Mech.*, **173**, 431-471.

Warren F. W. G. (1960) Wave resistance to vertical motion in a stratified fluid, *J. Fluid Mech.*, **7**, 209-229.

Weil J. C. (1988) Plume rise, *Lectures on air pollution modeling*, Editors, Venkatram A. and Wyngaard J. C., 119-166.

Yih C. S. (1977) *Fluid mechanics*, West River Press, 3530 West Huron River Drive, Ann Arbor, Michigan 48103, USA. xviii+pp.622.

Zhang X. and Ghoniem A. F. (1993) A computational model for the rise and dispersion of wind-blown, buoyancy driven plumes, Part I, Neutral stratified case. *Atmos. Environ.*, (in press).

Appendix

On the level-off region of plume trajectory

In a stable atmosphere, the air density decreases with height. As a buoyant plume rises, it entrains ambient air and the plume volume-averaged density increases. When the plume reaches the maximum height, it loses its vertical momentum since most of its kinetic energy is transformed into gravitational potential energy. In the level-off region of a plume trajectory, a slight overshoot of the final height is often seen. However, more than one oscillation is infrequently observed (Briggs, 1975). The same strong damping of oscillations is exhibited by our numerical simulations. To explain this behavior, Warren (1960) studied the damping of oscillation of a rising axisymmetric thermal and suggested that the rapid damping of plume oscillation is due to "wave drag". In the following, we develop a simple model to explain this phenomenon.

We assume that the plume motion is steady; the ambient wind, U, is uniform and the atmosphere is linearly stratified. The plume is assumed to be a parcel with volume-averaged density and at the position of its mass center. We denote the coordinate in the wind direction by x^*, and the vertical distance above the equilibrium height by z^*. The vertical momentum equation, after incorporating the Boussinesq approximation, can be written as

$$U \frac{\partial w^*}{\partial x^*} = - \frac{\rho_p}{\rho_o} g \qquad \text{(A1)}$$

where w^* is the plume vertical velocity. The rate of change of the average density inside the plume is approximated as

$$\frac{d}{dt}(\rho_a + \rho_p) = \frac{\dot{m}_e}{A} \qquad \text{(A2)}$$

where ρ_a and ρ_p are the air density and plume deficient density, respectively; $\frac{\dot{m}_e}{A}$ is the influx of air per unit cross-sectional area into the plume due to entrainment. For a plume with larger deficient density, the entrainment is stronger, so that the influx of air into its core is higher. We parameterize this influx using an entrainment coefficient α:

$$\frac{\dot{m}_e}{A} = - \alpha \rho_p . \qquad \text{(A3)}$$

Realizing $\frac{\rho_p}{\rho_a} << 1$ and that the air density is vertically stratified, we can simplify equation (A2) and rewrite it as

$$U \frac{\partial \rho_p}{\partial x^*} + w^* \frac{d \rho_a}{d z^*} = - \alpha \rho_p \tag{A4}$$

Eliminating ρ_p from (A1) and (A4), we obtain

$$U^2 \frac{\partial^2 w^*}{\partial x^{*2}} + \alpha U \frac{\partial w^*}{\partial x^*} + N^2 w^* = 0 \tag{A5}$$

where $N^2 = - \frac{g}{\rho_o} \frac{d \rho_s}{d z^*}$ is the square of the Brunt-Väisälä frequency which characterizes the stability of the atmosphere. Writing the vertical displacement of plume from the equilibrium height as $\xi^* = \int w^* \, dt^*$, then (A5) becomes

$$\frac{\partial^2 \xi^*}{\partial x^{*2}} + \frac{\alpha}{U} \frac{\partial \xi^*}{\partial x^*} + \frac{N^2}{U^2} \xi^* = 0. \tag{A6}$$

The solution of (A4) gives the trajectory of the plume:

$$\xi^* (x^*) = \xi_o^* \, exp \left(- \frac{\alpha}{2 U} x^* \right) cos \left(\frac{N}{U} \sqrt{1 - \frac{\alpha^2}{4 N^2}} \; x^* \right). \tag{A7}$$

where the origin of x^* is chosen at the location where ξ^* reaches its maximum value, ξ_o^*. Clearly, this maximum amplitude is related to the vertical momentum of the plume when it first crosses the equilibrium height.

Discussion:

(1) The oscillation amplitude decays exponentially as the plume proceeds in the wind direction. The decay length scale is

$$L_d = \frac{2 U}{\alpha} \tag{A8}$$

which is longer for large ambient wind speed U or small entrainment coefficient α. L_d depends on N since α is a function of stratification although it does not appear explicitly in (A8). For large N, or strong vertical stratification, the atmosphere is stable, and we expect the plume

entrainment to be weak, α to be small and L_d to be long. Therefore, the decay length scale is longer for stronger ambient stratification.

(2) The spatial wavelength is

$$L_w = \frac{U}{N\sqrt{1-\frac{\alpha^2}{4N^2}}} \tag{A9}$$

which is longer for faster ambient wind speed, shorter for stronger stratification and weaker entrainment.

(3) The number of plume oscillations depends on the ratio of $3L_d$, the distance over which 95% of the maximum amplitude decays, and $2\pi L_w$, the wavelength of the oscillation,

$$n = \frac{3L_d}{2\pi L_w} = \frac{3}{2\pi}\frac{2N}{\alpha}\sqrt{1-\frac{\alpha^2}{4N^2}}. \tag{A10}$$

For longer decay length or shorter wavelength, more oscillations are expected. There are two extremes. (a) $\alpha=0$, i.e., no entrainment is involved, the plume moves as a pure, non-dissipative internal wave. In this case, which corresponds to a passive plume in an internal wave field, we have an infinite number of oscillations. (b) $\alpha = 2N$, very large entrainment is involved and no oscillations occur. It is interesting to note that n is independent of the wind speed.

Generally, for $0 < \alpha/2N < 1$, the number of oscillations is finite and small if entrainment is large. The dependence of n on $\alpha/2N$ is shown on figure A1.

Figure Captions

Figure 1. Schematic drawing showing the generation of vorticity along the plume interface and in the surrounding, when atmosphere stratification is finite.

Figure 2. The computational domain in the cross-wind section at time $t = 0$, showing the discretization of the plume-air interface and the surrounding into transport elements. The air density profile is shown on the right-hand side.

Figure 3. The trajectories of the plume center in a linearly stratified atmosphere. Open symbols depict the numerical simulation results for four different buoyancy ratios. The extended two-thirds law is shown by solid lines for the same cases.

Figure 4. The equivalent radius of the plume cross section versus the plume rise for different buoyancy ratios. Numerical results are shown by open symbols while the integral relations are depicted by solid lines.

Figure 5. The change of the plume vertical width, defined in terms of the maximum vertical extension of the plume cross section, along the downwind distance.

Figure 6. The variation of the plume horizontal width, described by the maximum crosswind horizontal extension, along the downwind distance.

Figure 7. The total circulation generated at the plume-air interface on the right half of the plume cross section as a function of the downwind distance.

Figure 8. The total circulation generated in the background on the right half of the plume cross section as a function of the downwind distance.

Figure 9. The length of the plume circumference along the downwind distance.

Figure 10. The terminal or equilibrium height of a buoyant plume rising in a linearly stratified atmosphere as a function of the buoyancy ratio.

Figure 11. The evolution of the plume cross section, depicted in terms of the density contours, at different downwind locations for the case of $B=12.5$. All frames are from $y=0.0$ to $y=7.0$ and $z=23.0$ to $z=30.0$.

Figure 12. Contours of (a) the plume density, (b) vorticity, (c) the background density and (d) the velocity vectors in the plume cross section at $x = 4$ for a strongly stratified atmosphere, $B=12.5$. All frames are from $y=0.0$ to $y=6.0$ and $z=24$ to $z=30$.

Figure 13. Contours of (a) the plume density, (b) vorticity, (c) the background density and (d) the velocity vectors in the plume cross section at $x = 14$ for a strongly stratified atmosphere, $B=12.5$. All frames are from $y=0.0$ to $y=6.0$ and $z=24$ to $z=30$.

Figure A1. Number of oscillations near the equilibrium height as a function of $\alpha/2N$.

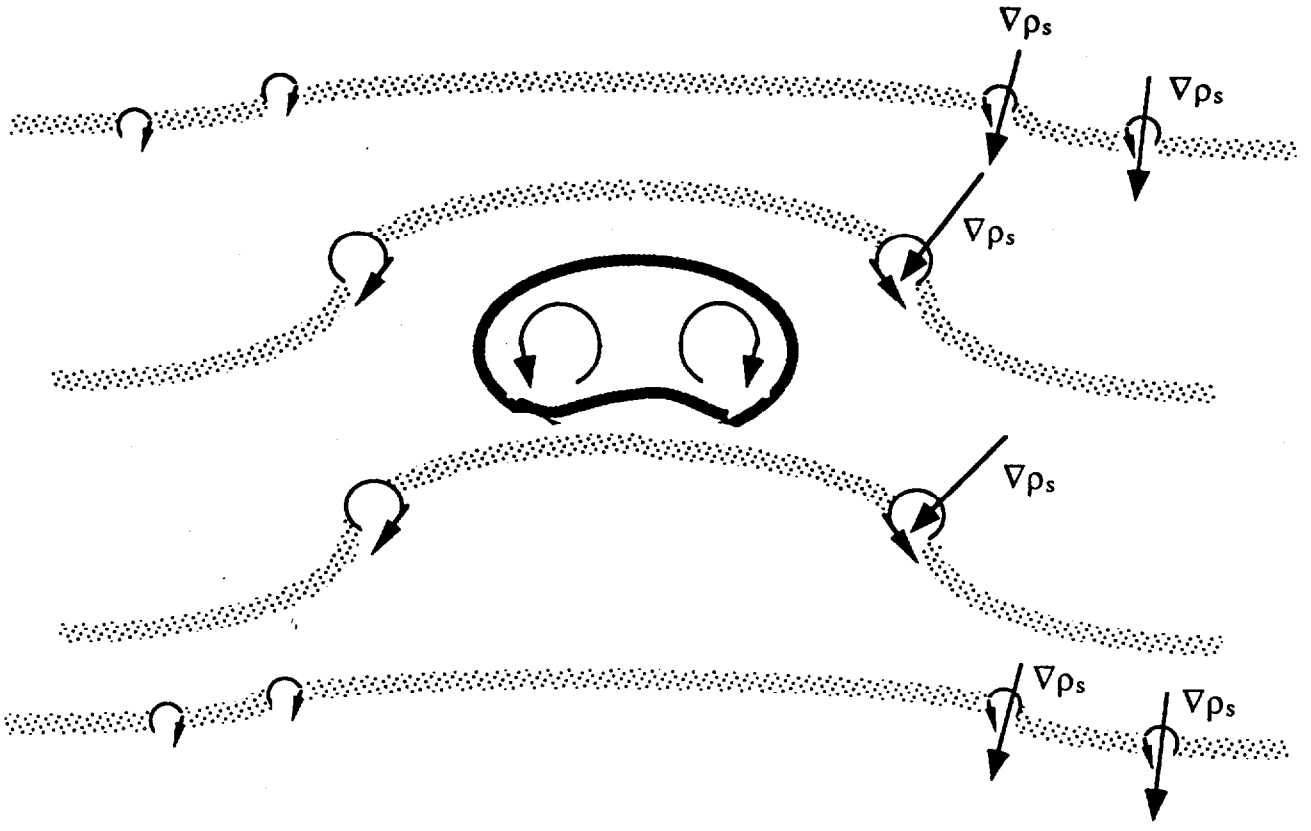
$\nabla\rho_s$
$\nabla\rho_s$
$\nabla\rho_s$
$\nabla\rho_s$
$\nabla\rho_s$
$\nabla\rho_s$

Figure 1

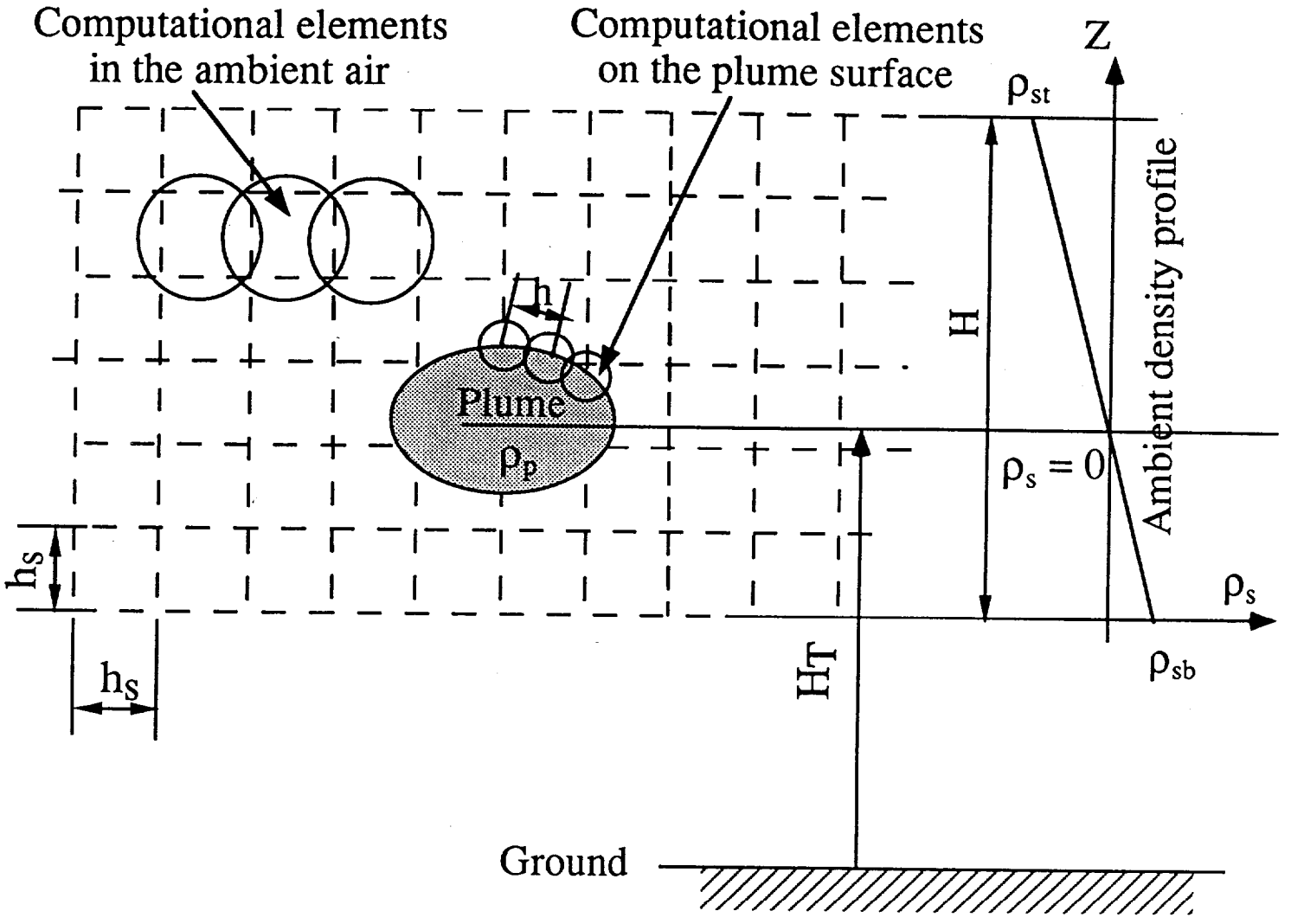
Computational elements
in the ambient air
Computational elements
on the plume surface
Z
ρ_{st}
h
H
Plume
ρ_p
$\rho_s = 0$
Ambient density profile
h_s
ρ_s
h_s
H_T
ρ_{sb}
Ground

Figure 2

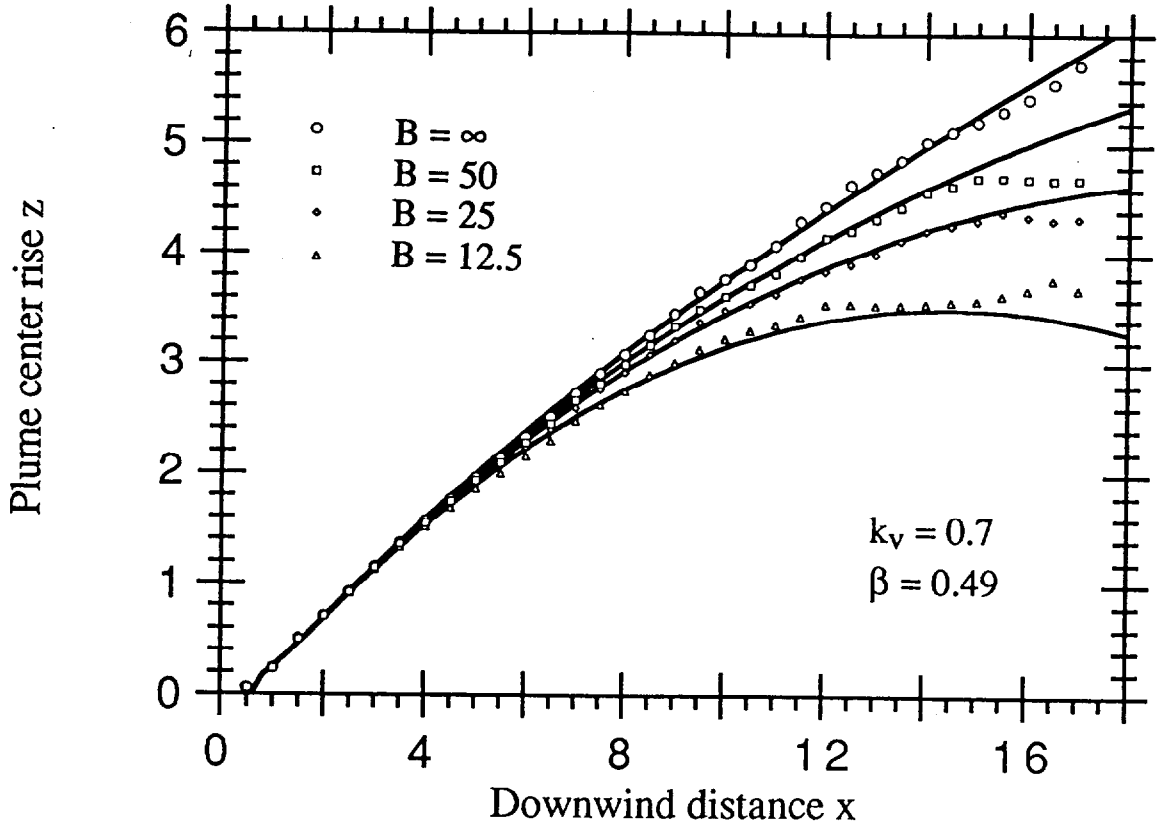
Plume center rise z
6
5
4
3
2
1
0
B = ∞
B = 50
B = 25
B = 12.5
$k_V = 0.7$
$\beta = 0.49$
0
4
8
12
16
Downwind distance x

Figure 3

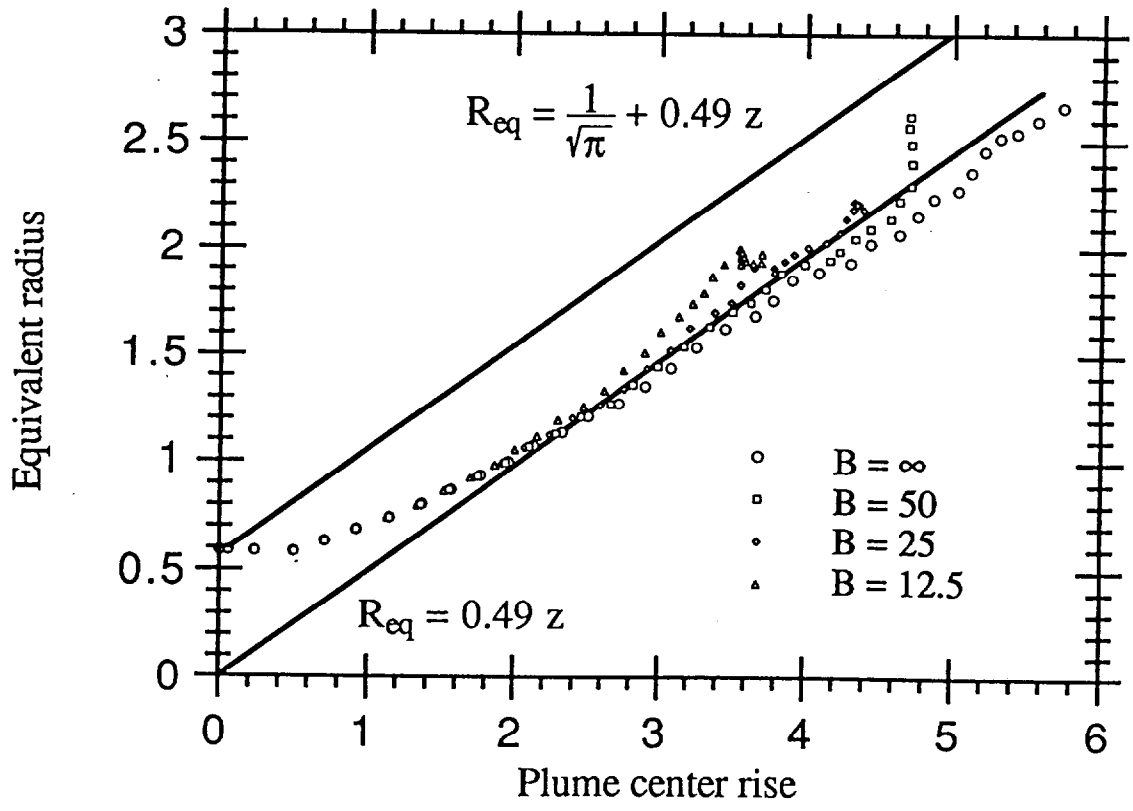
Equivalent radius
Plume center rise
$R_{eq} = \frac{1}{\sqrt{\pi}} + 0.49\ z$
$R_{eq} = 0.49\ z$
B = ∞
B = 50
B = 25
B = 12.5
0
0.5
1
1.5
2
2.5
3
0
1
2
3
4
5
6

Figure 4

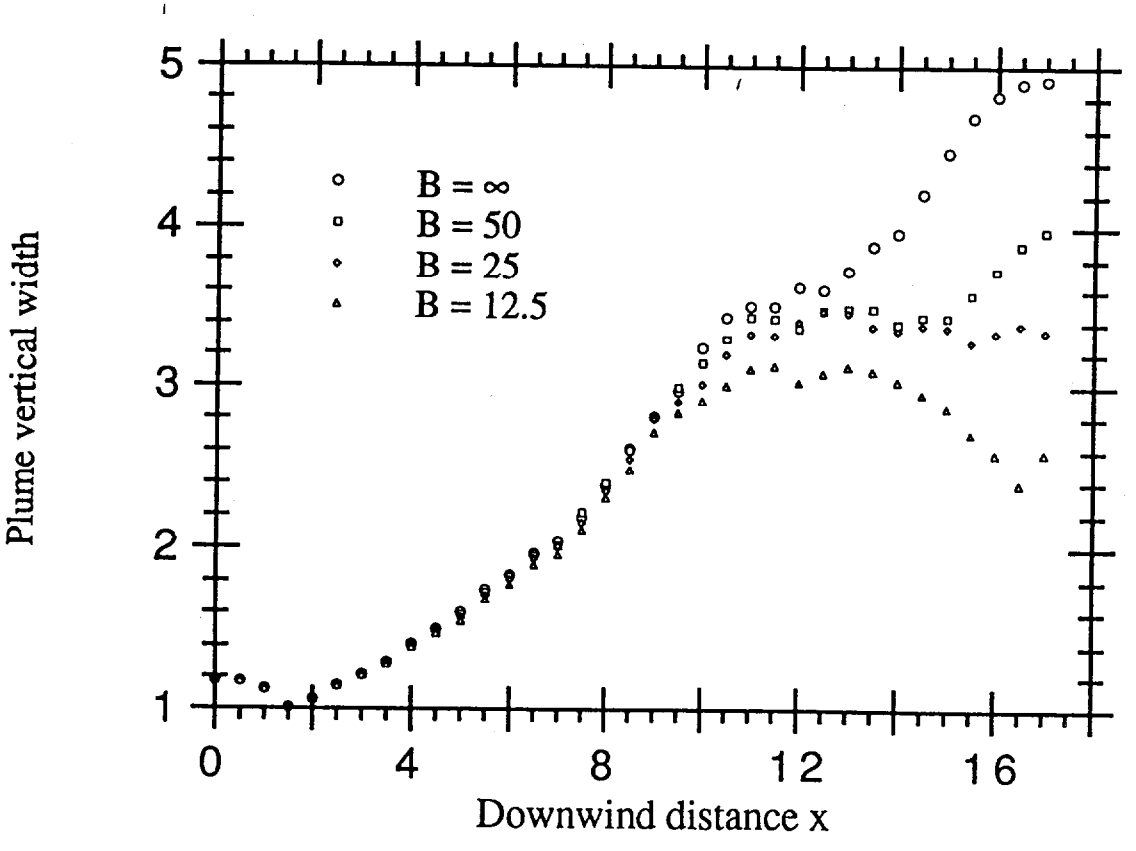
Plume vertical width
5
4
3
2
1
0
4
8
12
16
Downwind distance x
B = ∞
B = 50
B = 25
B = 12.5

Figure 5

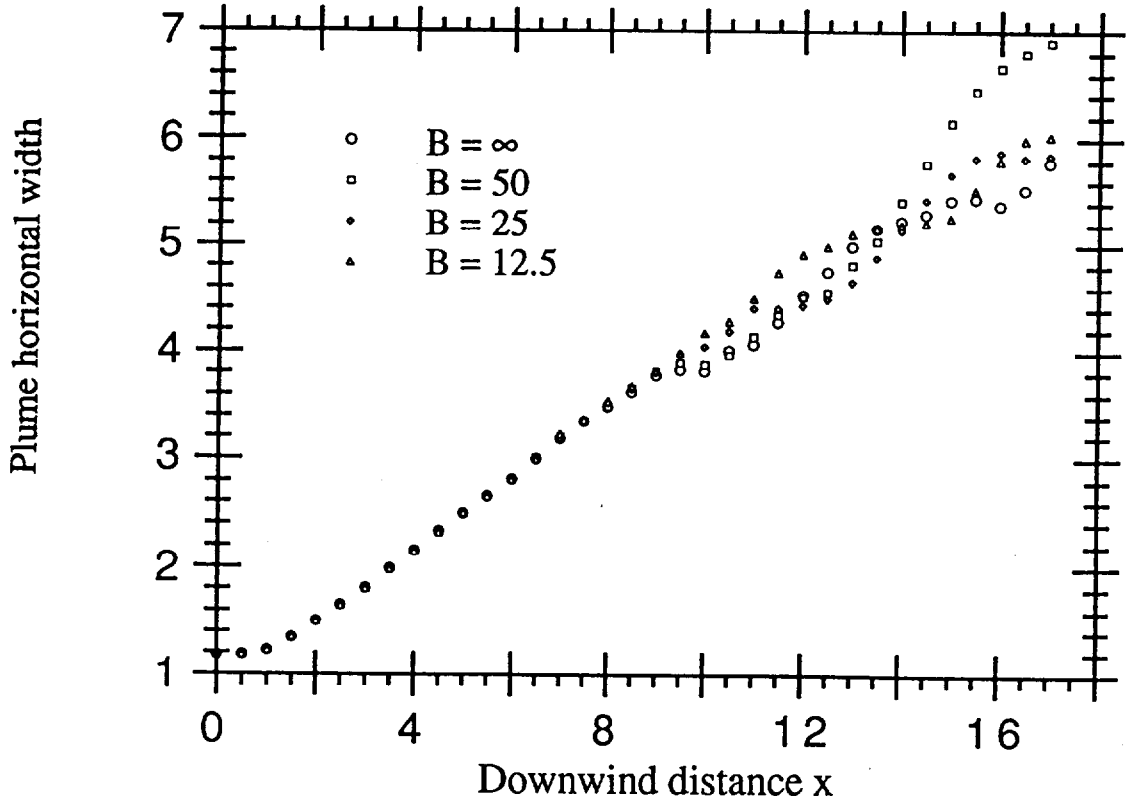
Plume horizontal width
7
6
5
4
3
2
1
B = ∞
B = 50
B = 25
B = 12.5
0
4
8
12
16
Downwind distance x

Figure 6

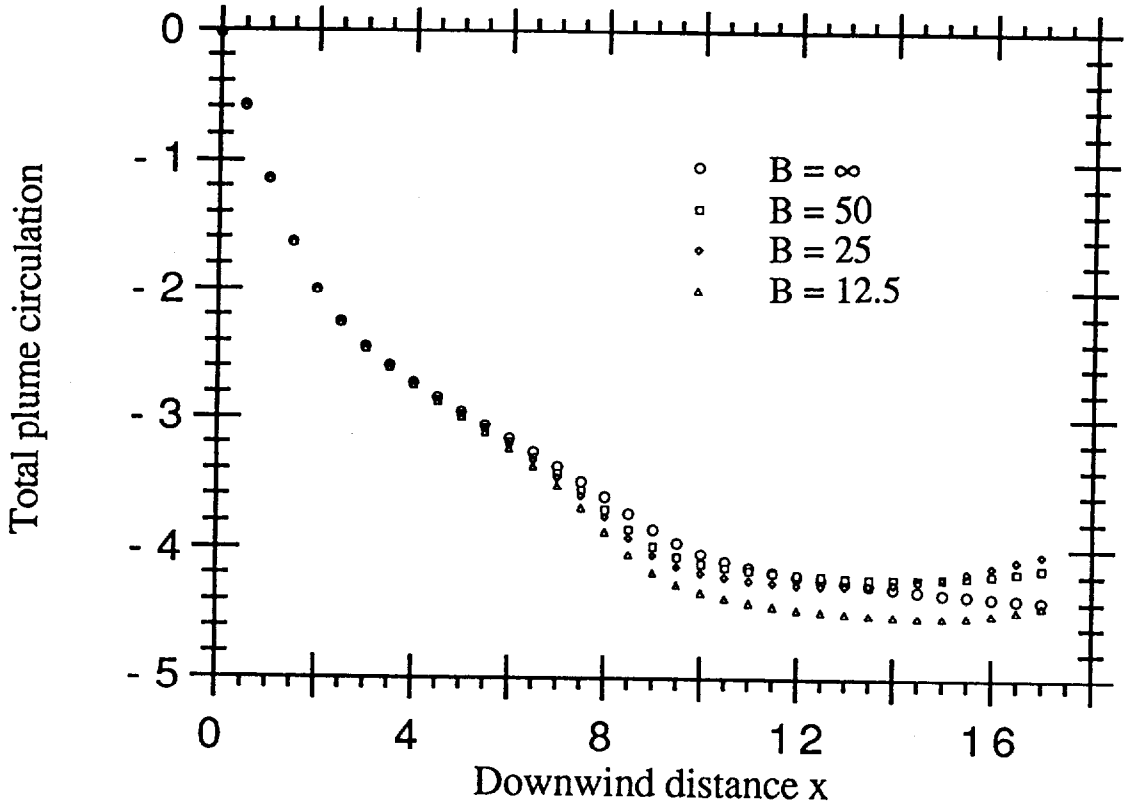
0
- 1
- 2
- 3
- 4
- 5
Total plume circulation
B = ∞
B = 50
B = 25
B = 12.5
0
4
8
12
16
Downwind distance x

Figure 7

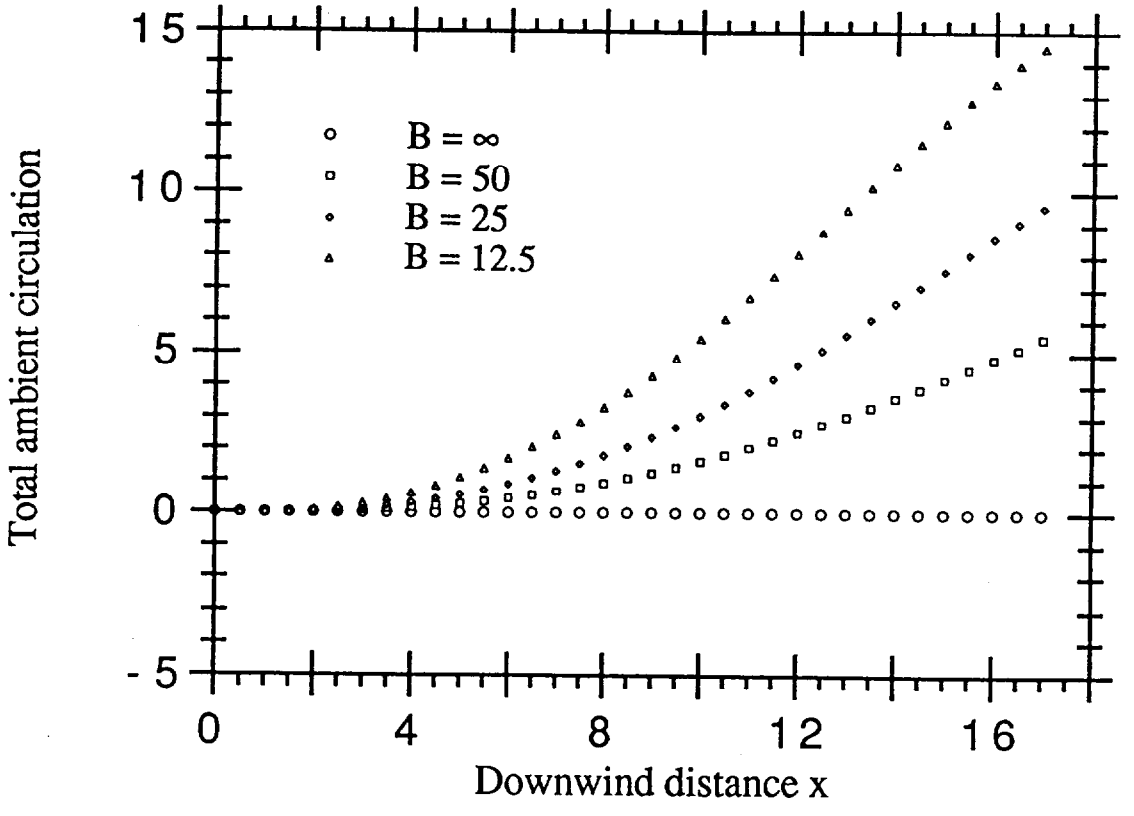
15
10
5
0
- 5
0
4
8
12
16
B = ∞
B = 50
B = 25
B = 12.5
Total ambient circulation
Downwind distance x

Figure 8

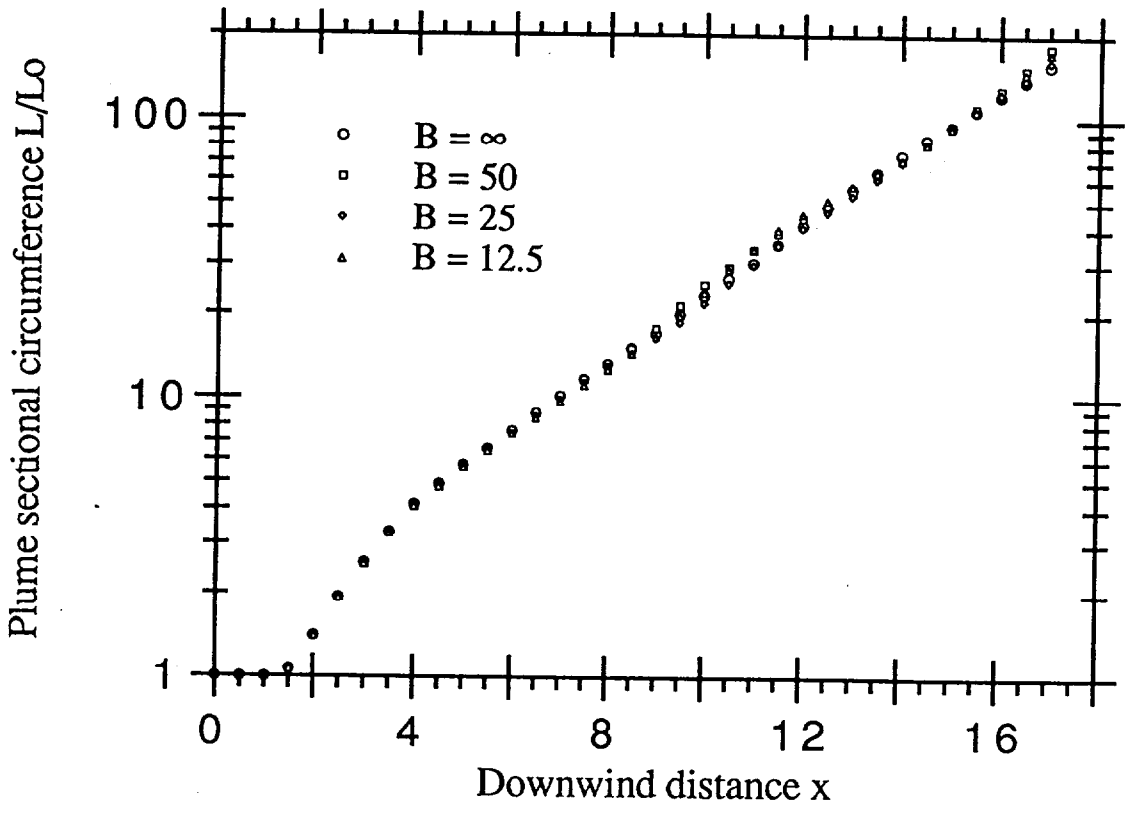
Plume sectional circumference L/Lo
100
10
1
0
4
8
12
16
Downwind distance x
B = ∞
B = 50
B = 25
B = 12.5

Figure 9

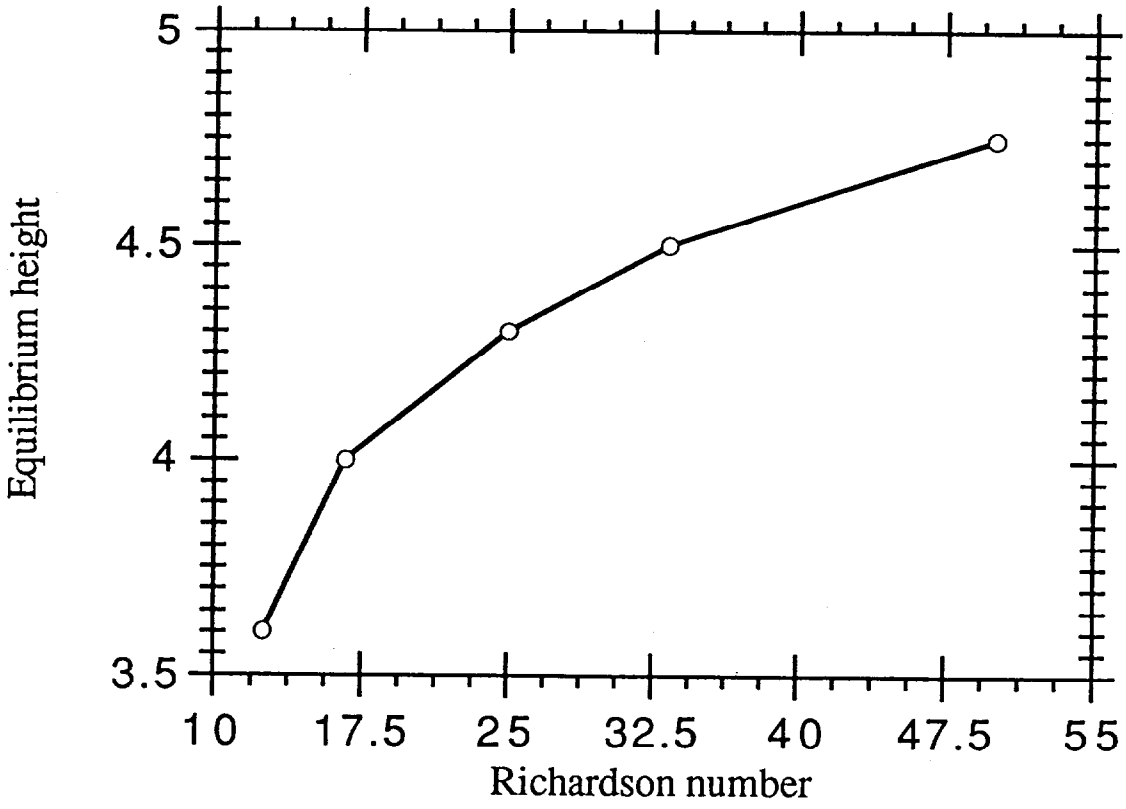
5
4.5
4
3.5
Equilibrium height
10
17.5
25
32.5
40
47.5
55
Richardson number

Figure 10

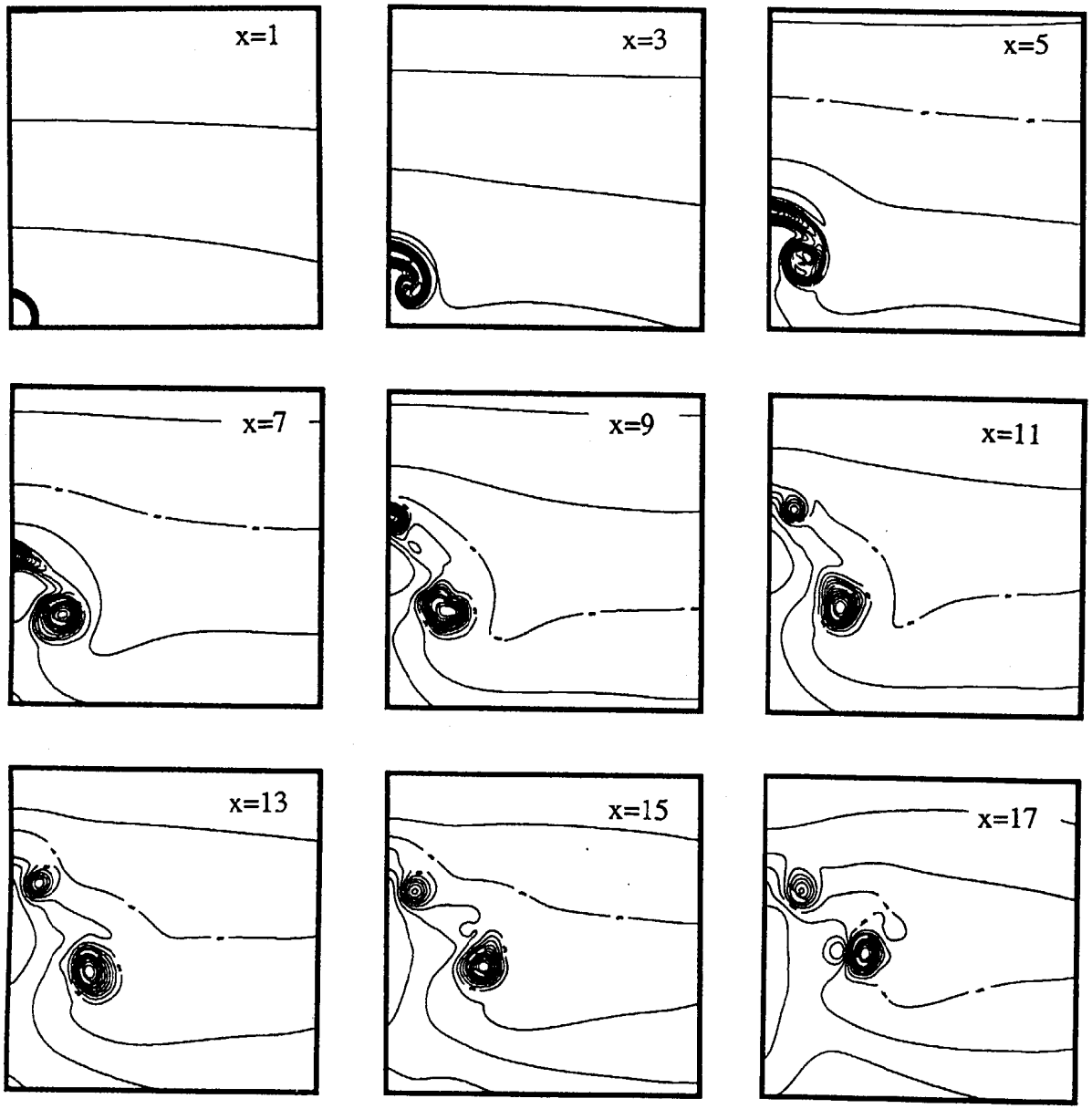
x=1
x=3
x=5
x=7
x=9
x=11
x=13
x=15
x=17

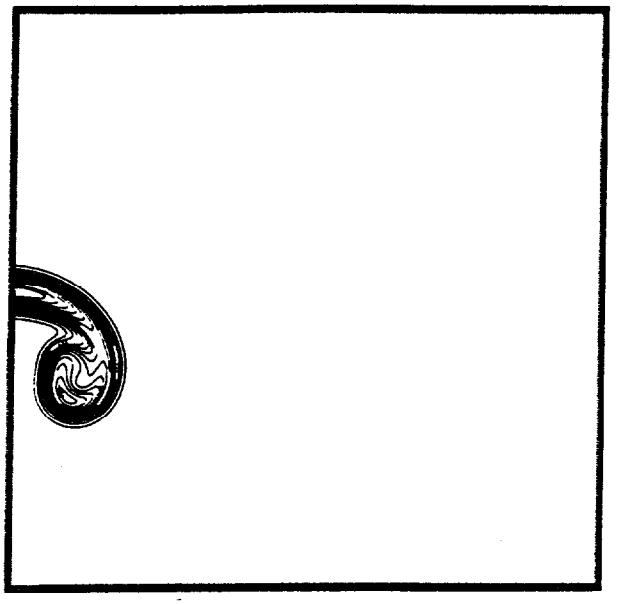

(a)

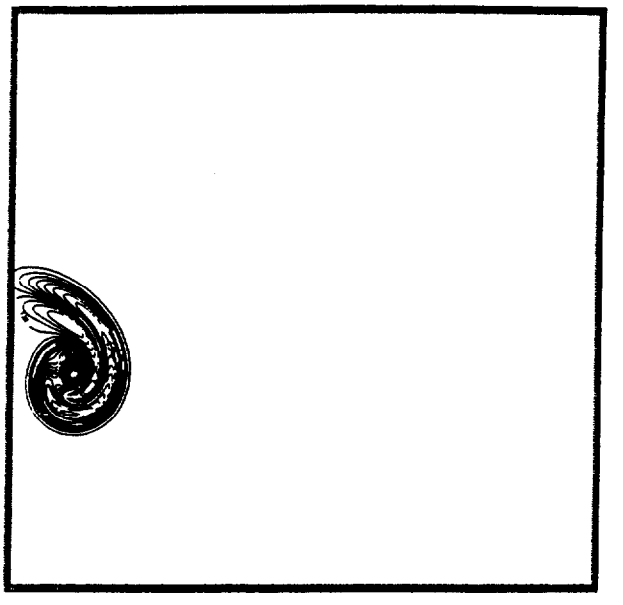

(b)

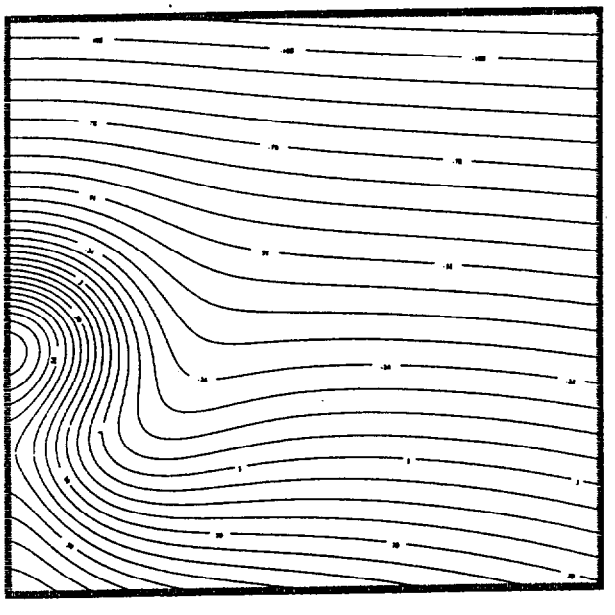

(c)

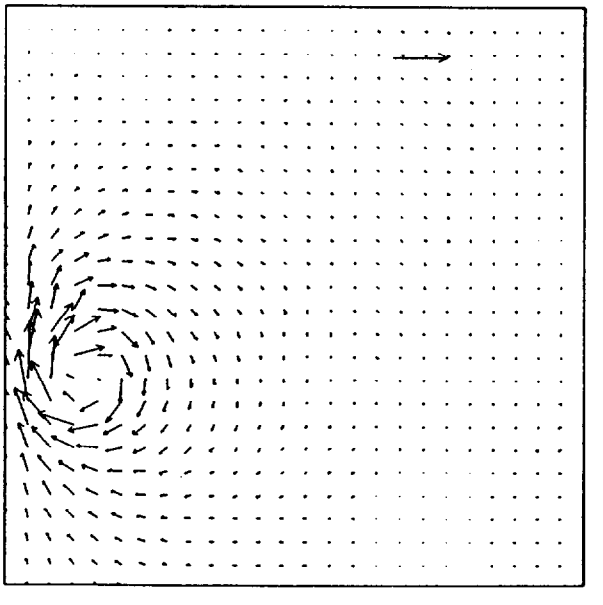

(d)

Figure 12

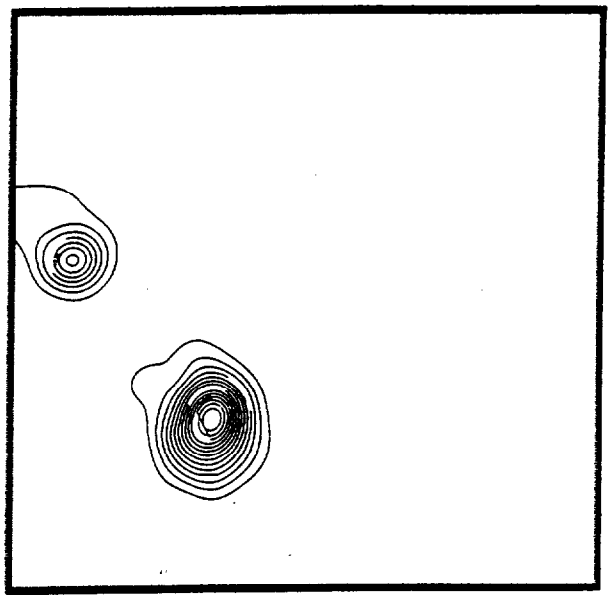

(a)

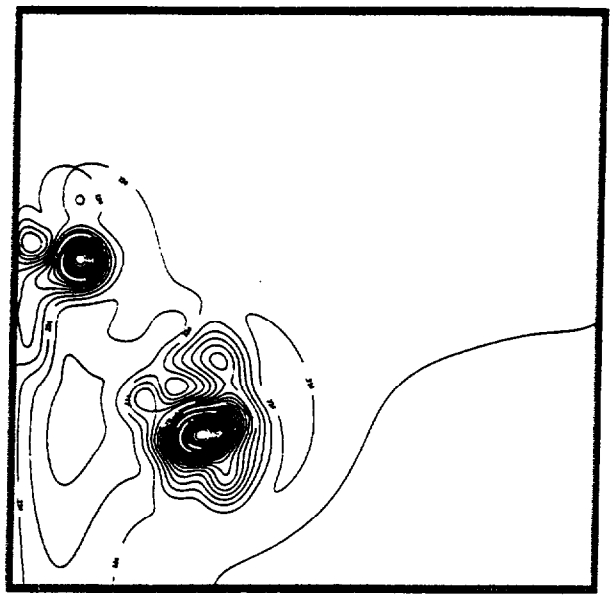

(b)

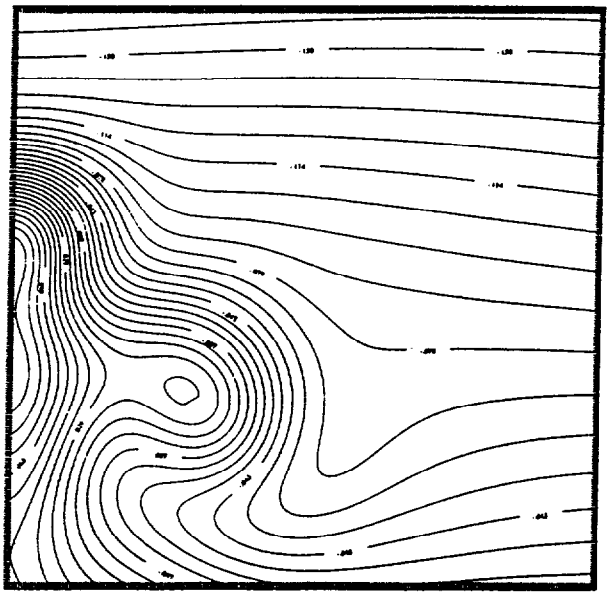

(c)

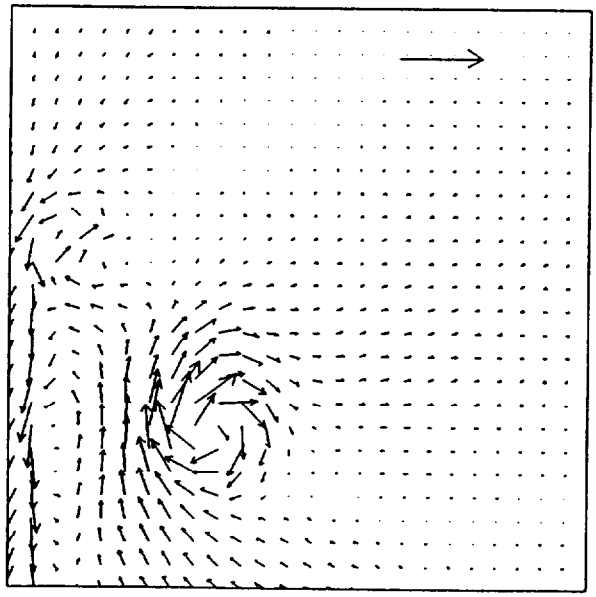

(d)

Figure 13

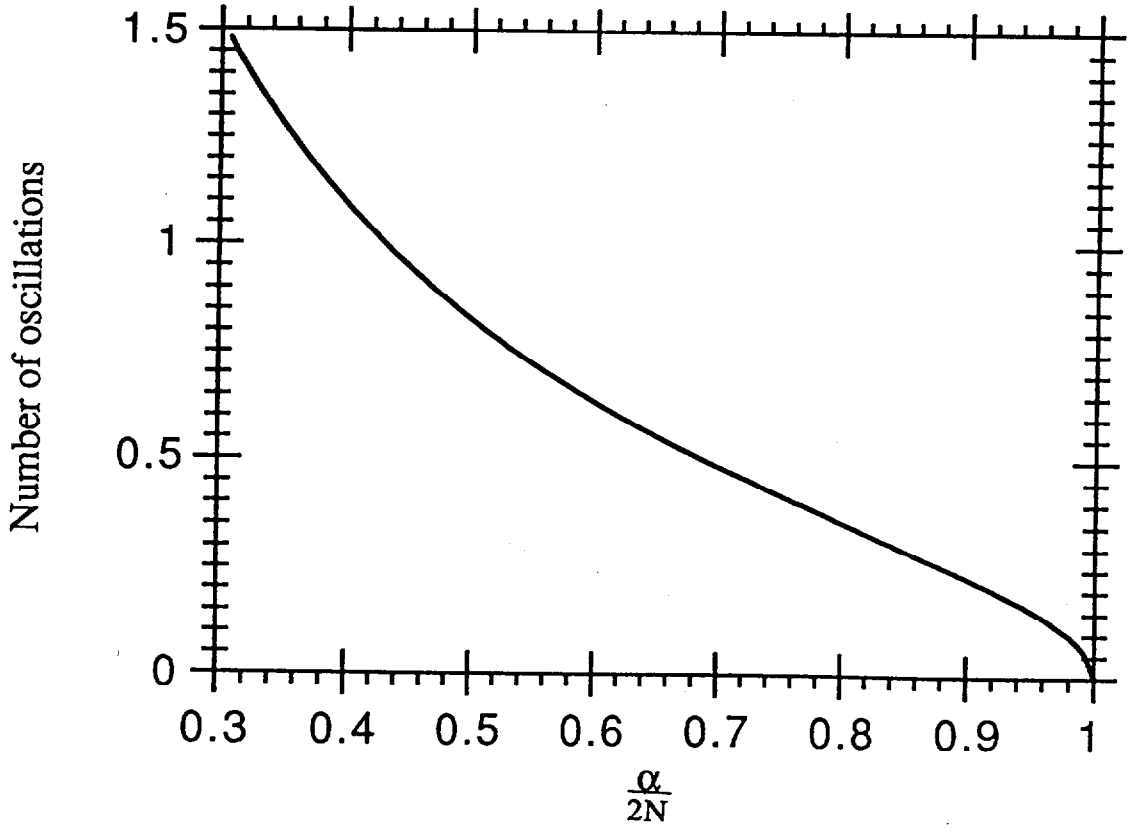

Figure A1

NIST-114
(REV. 9-92)
ADMAN 4.09

U.S. DEPARTMENT OF COMMERCE
NATIONAL INSTITUTE OF STANDARDS AND TECHNOLOGY

MANUSCRIPT REVIEW AND APPROVAL

(ERB USE ONLY)
ERB CONTROL NUMBER | DIVISION
PUBLICATION REPORT NUMBER: NIST-GCR-93-637 | CATEGORY CODE
PUBLICATION DATE: December 1993 | NUMBER PRINTED PAGES

INSTRUCTIONS: ATTACH ORIGINAL OF THIS FORM TO ONE (1) COPY OF MANUSCRIPT AND SEND TO: THE SECRETARY, APPROPRIATE EDITORIAL REVIEW BOARD.

TITLE AND SUBTITLE (CITE IN FULL)

A Computational Model for the Rise and Dispersion of Wind-Blown, Buoyancy-Driven Plumes Part II. Linearly Stratified Atmosphere

CONTRACT OR GRANT NUMBER: 60NANB0D1036

TYPE OF REPORT AND/OR PERIOD COVERED: Final Report

AUTHOR(S) (LAST NAME, FIRST INITIAL, SECOND INITIAL)

Xiaoming Zhang and Ahmed F. Ghoniem

PERFORMING ORGANIZATION (CHECK (X) ONE BOX)

[ ] NIST/GAITHERSBURG
[ ] NIST/BOULDER
[ ] JILA/BOULDER

LABORATORY AND DIVISION NAMES (FIRST NIST AUTHOR ONLY)

SPONSORING ORGANIZATION NAME AND COMPLETE ADDRESS (STREET, CITY, STATE, ZIP)

U.S. Department of Commerce
National Institute of Standards and Technology
Gaithersburg, MD 20899

RECOMMENDED FOR NIST PUBLICATION

[ ] JOURNAL OF RESEARCH (NIST JRES)
[ ] J. PHYS. & CHEM. REF. DATA (JPCRD)
[ ] HANDBOOK (NIST HB)
[ ] SPECIAL PUBLICATION (NIST SP)
[ ] TECHNICAL NOTE (NIST TN)
[ ] MONOGRAPH (NIST MN)
[ ] NATL. STD. REF. DATA SERIES (NIST NSRDS)
[ ] FEDERAL INF. PROCESS. STDS. (NIST FIPS)
[ ] LIST OF PUBLICATIONS (NIST LP)
[ ] NIST INTERAGENCY/INTERNAL REPORT (NISTIR)
[ ] LETTER CIRCULAR
[ ] BUILDING SCIENCE SERIES
[ ] PRODUCT STANDARDS
[X] OTHER NIST-GCR

RECOMMENDED FOR NON-NIST PUBLICATION (CITE FULLY) [ ] U.S. [ ] FOREIGN

PUBLISHING MEDIUM

[ ] PAPER [ ] CD-ROM
[ ] DISKETTE (SPECIFY)
[ ] OTHER (SPECIFY)

SUPPLEMENTARY NOTES

ABSTRACT (A 1500-CHARACTER OR LESS FACTUAL SUMMARY OF MOST SIGNIFICANT INFORMATION. IF DOCUMENT INCLUDES A SIGNIFICANT BIBLIOGRAPHY OR LITERATURE SURVEY, CITE IT HERE. SPELL OUT ACRONYMS ON FIRST REFERENCE.) (CONTINUE ON SEPARATE PAGE, IF NECESSARY.)

A multi-dimensional computational model of wind-blown, buoyancy-driven flows is applied to study the effect of atmospheric stratification on the rise and dispersion of plumes. The model utilizes Lagrangian transport elements, distributed in the plane of the plume cross section normal to the wind direction, to capture the evolution of the vorticity and density field, and another set of elements to model the dynamics in the atmosphere surrounding the plume. Solutions are obtained for a case in which atmospheric density changes linearly with height. Computational results show that, similar to the case of a neutrally stratified atmosphere, the plume acquires a kidney-shaped cross section which persists for a long distance downstream the source and may bifurcate into separate and distinct lumps. Baroclinic vorticity generated both along the plume boundary and in the surroundings are used to explain the origin of the distortion experienced by the plume and inhibiting effect of a stratified atmosphere, respectively. The vorticity within the plume cross section forms two large-scale coherent eddies which are responsible for the plume motion and the entrainment.

KEY WORDS (MAXIMUM 9 KEY WORDS; 28 CHARACTERS AND SPACES EACH; ALPHABETICAL ORDER; CAPITALIZE ONLY PROPER NAMES)

buoyant flows; computation; entrainment; fire phases; large fires; simulation; urban fires; wildland fires; wind effects

AVAILABILITY

[X] UNLIMITED
[ ] FOR OFFICIAL DISTRIBUTION. DO NOT RELEASE TO NTIS.
[ ] ORDER FROM SUPERINTENDENT OF DOCUMENTS, U.S. GPO, WASHINGTON, D.C. 20402
[X] ORDER FROM NTIS, SPRINGFIELD, VA 22161

NOTE TO AUTHOR(S) IF YOU DO NOT WISH THIS MANUSCRIPT ANNOUNCED BEFORE PUBLICATION, PLEASE CHECK HERE. [ ]

ELECTRONIC FORM